551.515.2

NEW ZEALAND METEOROLOGICAL SERVICE

TECHNICAL NOTE 231

A DIAGNOSTIC INVESTIGATION OF THE BEHAVIOUR OF TROPICAL CYCLONE NORMAN

K.E. Trenberth

Issued for limited distribution by:

The Director
New Zealand Meteorological Service
P.O. Box 722
WELLINGTON.

27 September 1977

THE NEW ZEALAND METEOROLOGICAL SERVICE

A DIAGNOSTIC INVESTIGATION OF THE BEHAVIOUR OF TROPICAL CYCLONE NORMAN

Abstract

The behaviour of tropical storm Norman is investigated using a diagnostic synoptic approach with the aim of determining the main factors governing the movement of the storm. In preparing detailed analyses, difficulties were encountered through the lack of observations and the occurrence of transient sub-synoptic scale features. These features were accompanied by spiral cloud bands, and may have been internal inertia-gravity waves, but their presence made the few available observations unrepresentative of the large-scale geostrophic flow.

The contributions to thickness and vorticity changes from advection, latent heating, and friction were evaluated and compared with the observed 12-hour changes. The mid-tropospheric vertical motions were deduced from the discrepancy, subject to residual errors arising from the analyses, assumptions made, and neglected terms. Subjective comparison with satellite pictures showed sufficient agreement to allow the main processes to be identified. The thickness equation proved more useful than the vorticity equation for this purpose.

Strong upward motions south and southeast of Norman were mostly due to warm advection supplemented by latent heat release. The resulting convergence continually generated cyclonic vorticity and caused the vortex to move southwards. The presence of strong upward motions, as indicated by clouds in satellite pictures, should be useful as a means of assessing the effects of development on the movement of a storm.

1. Introduction

Tropical cyclone Norman was identified and named on 9 March 1977 near 11°S 166°E. It initially moved southwards, then southeastwards for a time towards the area of responsibility of New Zealand forecasters. By the time it had reached 25°S 170°E at 2000 G.M.T. on 18 March it had resumed its southward movement. Its full track is given in Fig. 1. Prognoses of the track of the storm from about 0000 GMT 19 March favoured a trend for more southeastward movement, whereas, in fact, it continued to move almost due south. The main basis for the forecast of more easterly movement was a qualitative assessment of the 'steering field' which appeared to be northwesterly. In this paper a diagnostic synoptic study is made of the behaviour of Norman in order to determine the main factors in the storm's movement for the period 0000 GMT 19 to 21 March.

For much of its life, the central pressure of Norman was just below 990 mb and gale force winds were recorded in its vicinity, but it did not develop beyond that stage. The storm was responsible for about 50 mm of rain in northern New Zealand over a 3 day period from 21 March.

2. Method

Unfortunately, the storm travelled through an area that is poorly observed, and many details of the analyses could not be properly resolved.

The approach used is very simplistic and, in hindsight, is not to be recommended in general. The main working charts used by forecasters in the New Zealand Meteorological Service are those showing the 1000 mb (or surface), 500 mb, 300 mb and the thickness fields. Therefore, in order that the results of this study might be useful for subjective assessments of similar situations, a diagnostic model was formulated using only parameters defined at the 1000 and 500 mb levels. In effect this method uses a two-layer model and will be limited to resolving only large-scale effects. The 1000 mb, 1000-500 mb thickness and 500 mb fields were carefully analysed by hand and grid-point values read off and coded for computer processing. This enabled the actual rates of change of different parameters to be estimated and compared with those based on computations of advection, development, diabatic heating and friction.

The grid used was a $\frac{1}{2}$ inch square grid on 1:20 million scale stereographic projection, and this has a grid spacing of 205 km at 30°S. Calculations were made for a 12 by 12 grid with true north along 175°E. Results will be presented for the 10 by 10 interior points.

As the changes can be determined only between the main synoptic observation times (every 12 hours) we are effectively using a 12 hour time step. Therefore the fields must be heavily smoothed in order to ensure compatibility between rates of movement and the time and space scales. This also ensures that the main motions we shall be dealing with are quasi-geostrophic in nature. Details of the finite difference schemes and smoothing used are given in the appendices.

We use the quasigeostrophic vorticity equation

$$\frac{\partial \zeta}{\partial t} = -\underline{v} \cdot \nabla(\zeta + f) + f_0 \frac{\partial \omega}{\partial p} \qquad (1)$$

and thermodynamic equation

$$\frac{\partial}{\partial t}\frac{\partial \phi}{\partial p} = -\underline{v} \cdot \nabla \frac{\partial \phi}{\partial p} - \sigma\omega - \frac{\chi Q}{p} \qquad (2)$$

where $\zeta = \frac{1}{f_0}\nabla^2\phi$ is the geostrophic relative vorticity

f is the Coriolis parameter

f_0 is a constant value for f (taken at 30°S)

$\underline{V}$ is the horizontal non-divergent velocity vector

ω is the vertical p-velocity

p is the pressure

t is time

ϕ is geopotential

$\kappa = R/c_p$ where R is the gas constant and c_p is the specific heat at constant pressure

Q is the diabatic heating rate

$\sigma = -\frac{1}{\rho}\frac{\partial \ln \theta}{\partial p}$ is the static stability

ρ is the density

and θ is the potential temperature.

Using finite differences, it is possible to estimate the contributions from the most important terms, subject to largely unknown errors, except for those involving the mid-tropospheric vertical motions. Therefore we will assess the residual or unexplained contributions arising from the vertical motions, all neglected terms, assumptions made, and the inaccuracies in the analyses. If the latter three effects are sufficiently small, the resulting patterns should provide an estimate of the mid-tropospheric vertical motions which can be subjectively verified with satellite cloud pictures. In this way it may be possible to determine the dominant effects present. Note that the primary purpose is not to estimate the mid-tropospheric vertical motions, since that would be better done using the quasigeostrophic omega equation (or a more complete form, see Krishnamurti, 1968a), or kinematic method (Obrien 1970, Vincent et al. 1976).

We apply (1) at 750 mb to the 1000-500 mb layer, and define

$$\phi_{750} = \tfrac{1}{2}(\phi_{1000} + \phi_{500}).$$

$$\frac{\partial}{\partial t}\frac{1}{f_o}\nabla^2\left(\frac{\phi_{1000}+\phi_{500}}{2}\right) = -J\left(\frac{1}{f_o}\frac{(\phi_{1000}+\phi_{500})}{2}, \frac{1}{f_o}\nabla^2\frac{(\phi_{1000}+\phi_{500})}{2} + f\right) + f_o\frac{\omega_{1000}-\omega_{500}}{\Delta p} \qquad (3)$$

where $\Delta p = 500$ mb, and J is the Jacobian.

The thermodynamic equation is applied to the 1000-500 mb thickness field

$$\frac{\partial}{\partial t}\frac{\phi_{1000}-\phi_{500}}{\Delta p} = -J\left(\frac{1}{f_o}\,\frac{\phi_{1000}+\phi_{500}}{2}\,,\,\frac{\phi_{1000}-\phi_{500}}{\Delta p}\right)$$

$$-\sigma_{750}\,\frac{\omega_{1000}+\omega_{500}}{2} - \frac{\kappa\, Q_{750}}{p_{750}} \qquad (4)$$

The vertical motion at 1000 mb is assumed to be solely due to friction, since orographic influences are negligible in this area. If we assume the surface stress is given by

$$\underline{\tau}_o = \rho_o C_D \underline{V}_o \qquad (5)$$

where $\underline{V}o$ is the surface velocity, and C_D is the drag coefficient, then the vertical velocity at the top of the friction layer ω_F is given by

$$\omega_F = \frac{-\rho_o g C_D \zeta_o}{f_o} \qquad (6)$$

(Haltiner 1971, p 152). We take ω_{1000} to be ω_F but the surface vorticity, ζ_o, derived from geopotential heights using the geostrophic relation, will be a gross overestimate. For this case, surface winds reported by ships in the area of interest were a factor of 4 less than the geostrophic winds owing to both frictional and curvature effects.

This formulation is the same as that used by Trenberth (1973) in a numerical weather prediction model. The value of C_D reported there was .017 m s^{-1}, but revised analysis procedures (Trenberth 1977) have allowed this to be reduced to a more realistic value of .011 m s^{-1}. In this study, a further reduction by a factor of 4 is included to allow for the overestimate of ζ_o, and a value of C_D = .0025 m s^{-1} was used, which should provide a very conservative estimate of surface friction effects.

The main diabatic heating originates from latent heating and this is the only heating term we shall evaluate. We put

$$Q_{750} = r L \gamma_{750} \frac{g}{\Delta p} \qquad (7)$$

where,

L is the latent heat of vaporisation (=2.5x10^6J kg^{-1})

γ is the fraction of latent heat released in the layer (=0.9), and

r is the rainfall rate in mm s^{-1}, given by

$$r = \exp(13.8\,RH - 19.98) \qquad (8)$$

where RH is the mean relative humidity in the 1000-500 mb layer (Trenberth 1973, p. 15).

By substituting (6) into (3), and (6) and (7) into (4), all terms on the RHS of (3) and (4) can be evaluated except for ω_{500}. The actual rates of change of vorticity and thickness, on the LHS of (3) and (4), can be evaluated from the differences between the 0000 and 1200 GMT values. A comparison of these with the terms on the RHS averaged at 0000 and 1200 GMT then enables two quite separate estimates to be made of ω_{500}, which can be compared with each other and the satellite pictures. The degree of correspondence between them will indicate the importance of

(i) neglected terms - radiation, sensible heating, diffusion, internal friction, and all ageostrophic effects;

(ii) assumptions made - those in equations (5), (6) (7) and (8);

(iii) the accuracy of the analyses;

(iv) the accuracy of the finite differences, the vertical resolution, and method.

Since latent heating is always positive and radiative and other sources of cooling are neglected, there will be a bias toward upward motion in our estimates.

3. Analysed fields

Figure 2 shows the analysed 1000 mb and 500 mb height and 1000-500 mb thickness fields for 0000 GMT 19 to 21 March 1977. Also shown are nephanalyses from NOAA visible and infrared satellite pictures which are valid roughly 3 hours prior to the main synoptic observation time.

Relative humidity analyses were prepared based on the appearance of cloud in the satellite pictures (May and Kidson 1971) and rainfall rates were computed using (8). Observed rainfall at Raoul I. was confined to a trace on 20 and 21 March 1977 whereas the computed value of rainfall for the 2 days was 1 mm. At Norfolk I. the observed rainfall was 14 mm compared to the computed value of 4 mm. Rainfall at Kaitaia in northern New Zealand began at 1500 GMT 20 March and was computed to be 12 mm/day at 0000 GMT 21 March compared to the observed 4.5 mm/9hrs up to 0000 GMT and 14.0 mm in the next 12 hours. The maximum computed rainfall rate using the smoothed fields was 16 mm/day.

The rainfall totals for the three days on 21, 22 and 23 March at Kaitaia, Auckland Airport and Whenuapai were 49.9, 38.3 and 74.1 mm. With such natural variability present and bearing in mind that the computed values represent areas greater than a 200 km square the agreement is reasonable.

The analyses show the dominance of Norman in the 1000 mb field, yet its virtual absence at 500 mb. The lack of any high cloud near the vortex in the satellite pictures is

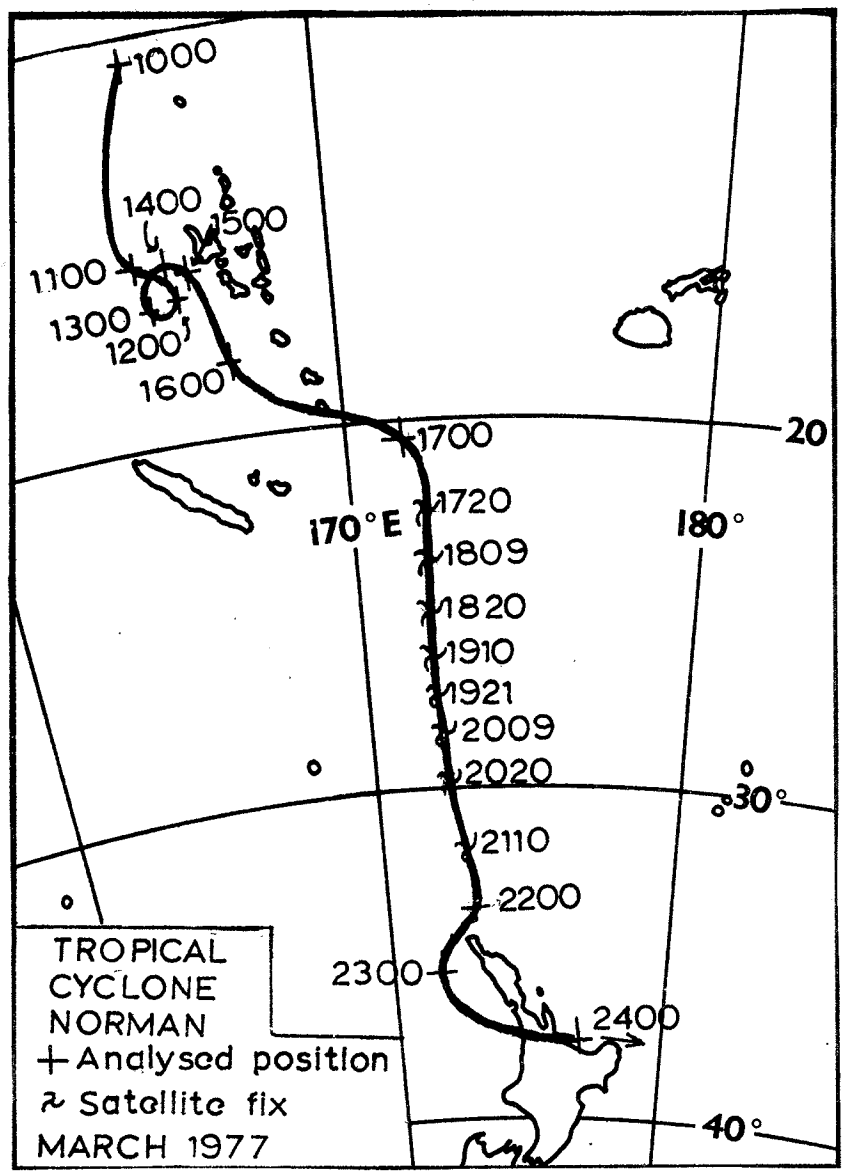

Fig. 1. The track of tropical cyclone Norman, March 1977. Times are shown as the date (first two figures) and hour (last two figures) in G.M.T.

Fig. 2 a,b,c.

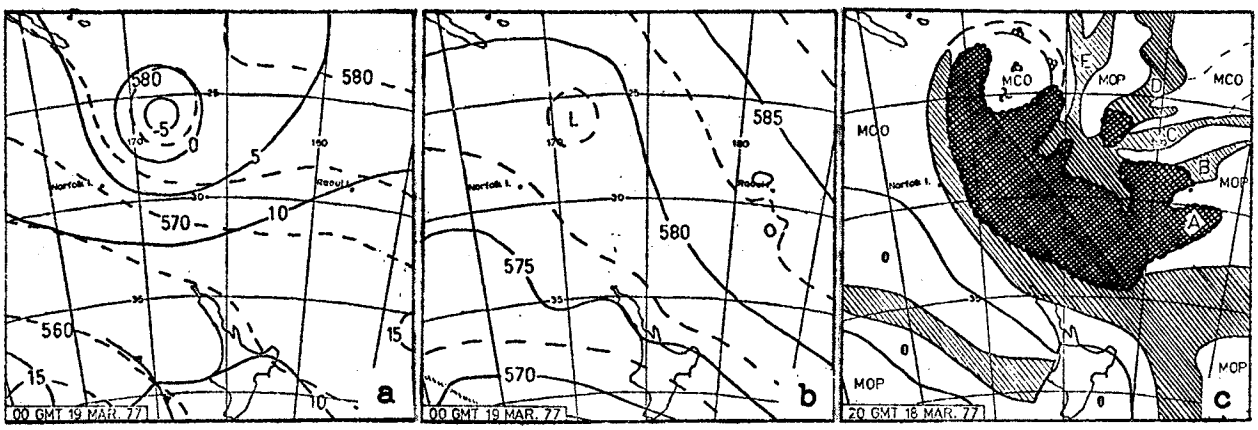

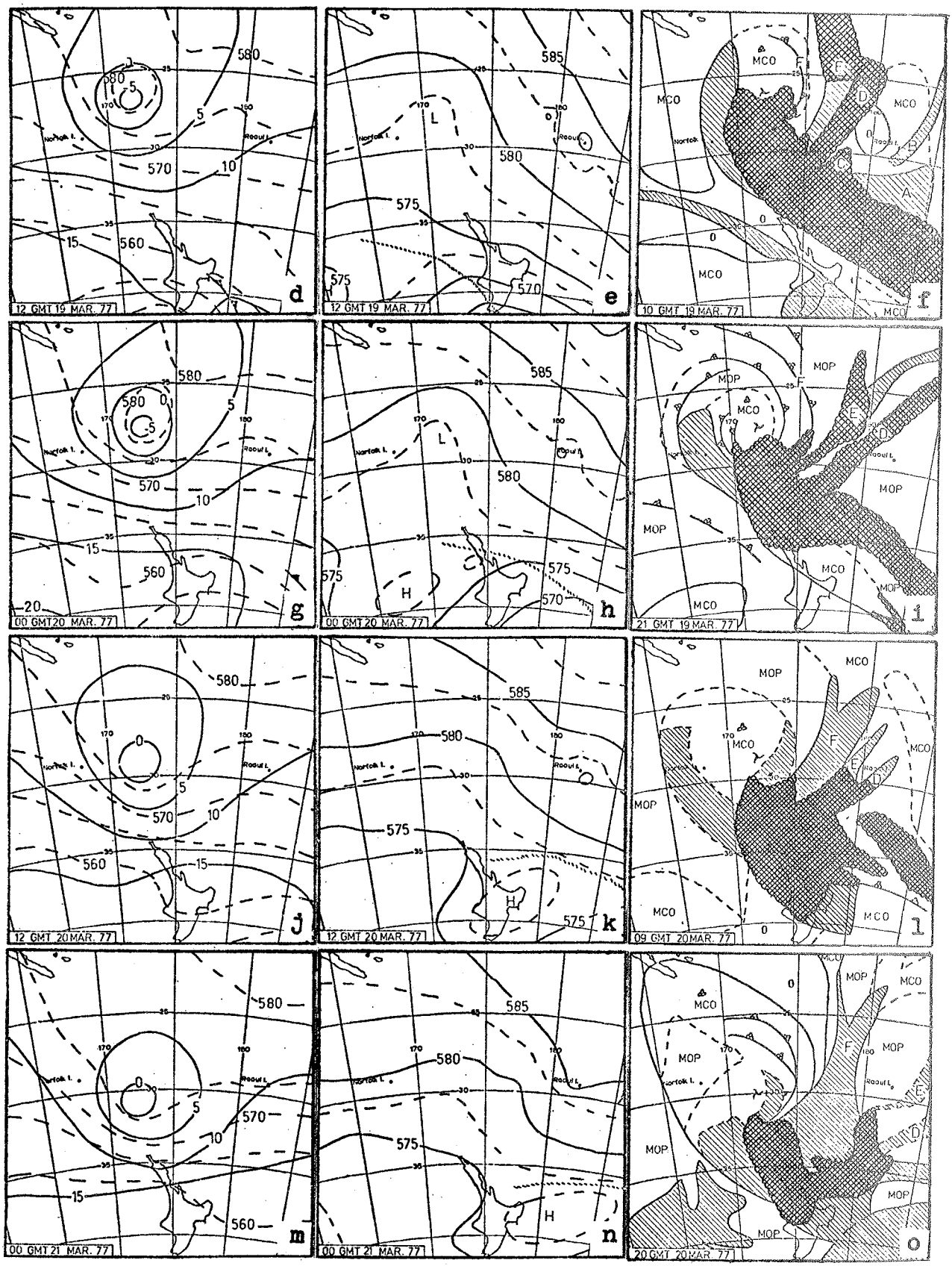

Fig. 2. Analyses of 1000 mb height and 1000-500 mb thickness contours; 500 mb height contours; and satellite mosaic nephanalyses; for 00 GMT 19 March (a), (b), (c); 12 GMT 19 March (d), (e), (f); 00 GMT 20 March (g), (h), (i); 12 GMT 20 March (j), (k), (l); and 00 GMT 21 March 1977 (m), (n), (o). In the nephanalyses, low level cloudy areas are shaded and areas of high and low level overcast are cross shaded.

consistent with this. The presence of a northwesterly 'steering current' seems fairly clear, and in fact many small scale features did move southeastwards, but not the main vortex. The other main feature of note is the very rapid movement of a front in the south Tasman Sea followed by anti-cyclogenesis. The main high at 500 mb moved fairly consistently throughout the period at 30 kt. However the surface anticyclone developed two centres between 40° and 45°S, south of the maps presented.

The preparation of the analyses was very difficult because of the poor data base and the dominance of very small scale features with relatively large amplitude. The main observing stations in the region are Raoul Is., Norfolk I. and Auckland, which lie about 1000 km apart, and it is therefore difficult to resolve the smaller scale features quantitatively, although they could be traced using satellite pictures.

Time sections of the events at these three stations were plotted. Assuming that features identified crossing an observation point can be extrapolated in position forward and backward in time, the time section should be equivalent to a cross section tangential to the large-scale flow at one instant. In this case, such a procedure was highly suspect owing to the short life times and rapid changes in character of the cloud bands accompanying the troughs, and consequently it was not possible to determine the details of the analyses in many areas by this method.

The small scale features in question were observed mainly in the mid-troposphere at Raoul I. There was little change in the surface pressure, lower or higher level winds, but 500 mb heights and winds fluctuated rapidly. These features did not occur at Norfolk I. Time sections at Raoul I. are given in Fig. 3 derived from 12 hour soundings showing (a) winds and dew point depression, and (b) isentropes. Figure 4 shows the sequence of 1000 mb, 700 mb and 500 mb heights. From these, the passage of several mid-tropospheric troughs and ridges can be seen, with changes in 500 mb heights and 1000-500 mb thickness of about 70 m. These features appeared to have a period of 28 hours at 700 mb or 36 hours at 500 mb. Their passage partly coincided with the movement of spiral cloud bands across the island, of which 6 were traceable, labelled A, B, C, D, E and F in Figs 2 and 4. The C-D-E series of bands appeared at times to be one complex cloud band, and F was also composed of several parts which were not individually traceable. The cloud bands were about 200 km apart and moved at a speed of 5 m s^{-1}. However, the bands were not all in existence at one time and each was most intense for only one day with a total lifetime of less than 2 days. They developed in the northeast sector of the storm, as they approached Raoul Island, but decayed rapidly after passing through. It implies that many small scale features were present which are lacking in the time sections in Figs 3 and 4, as analysed. For instance, an alternative hypothetical analysed sequence is also shown in Fig. 4 for 500 mb. It illustrates the problem known as aliasing, where the higher frequency wave is 'aliased' onto the smoothed curve as first analysed, and the exact period cannot be determined.

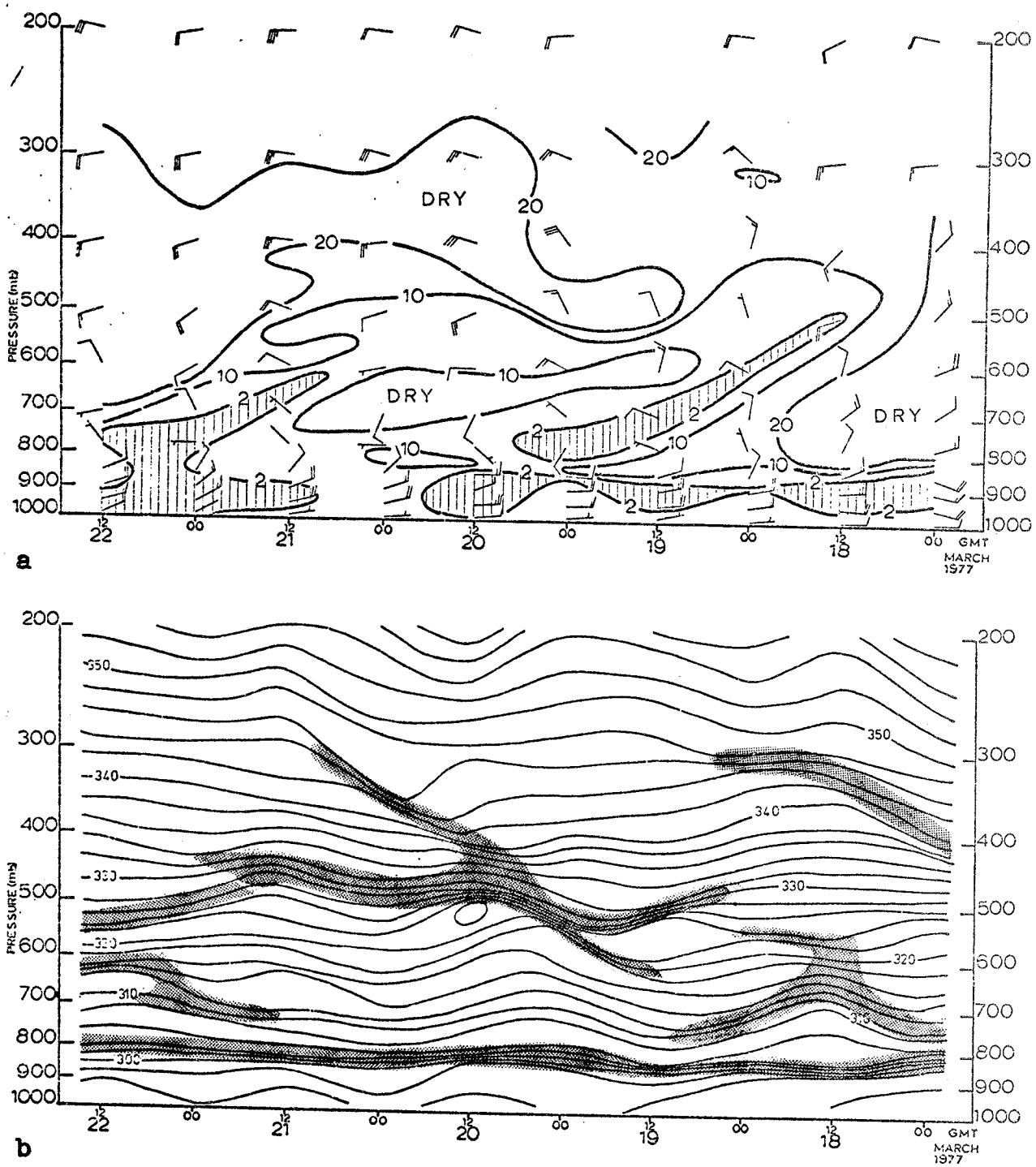

Fig. 3. Time sections at Raoul Is. for 18-22 March 1977,
(a) wind and dew point depression,
(b) isentropes.
Dew point depressions of less than 2° are shaded in (a), and in (b) the shading indicates the more stable layers.

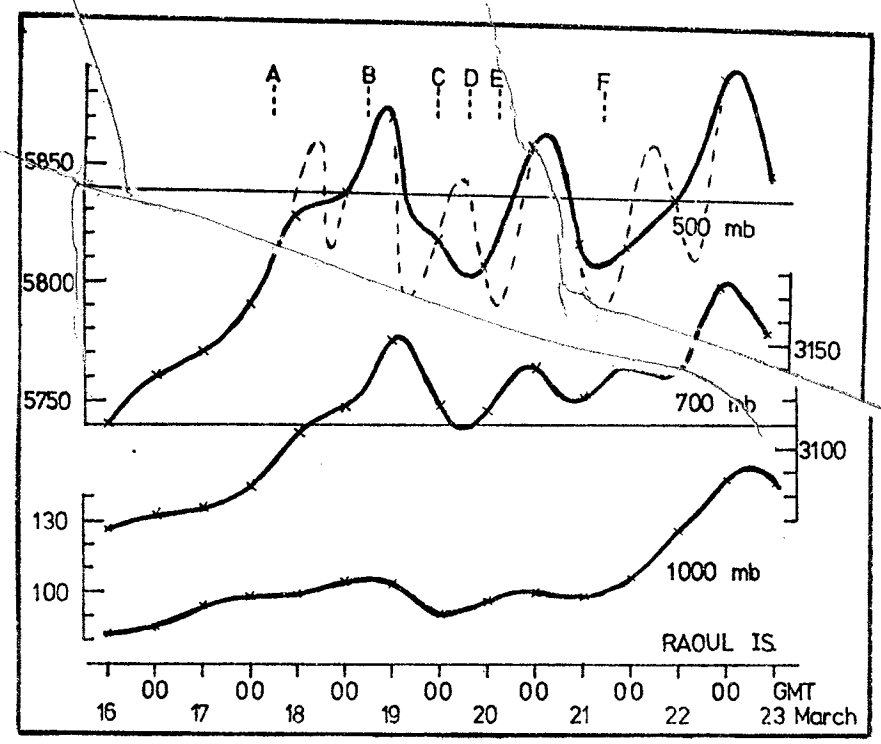

Fig. 4. Sequence of geopotential heights at Raoul Is at 1000, 700 and 500 mb. At 500 mb at alternative possible analysis of the sequence is indicated by the dashed line to illustrate unresolved aliasing problems.

The main stable layers are shaded in Fig. 3b and show regions where vertical motions have altered the static stability. The quasi-permanent trade wind inversion near 850 mb is prominent for the entire period, and a second inversion is present near 500 mb. Especially notable is the stable layer near 600 mb at 1200 GMT on the 18th which was followed by a tongue of moist air (Fig. 3a) and a backing of the wind, and progressed downwards to 800 mb by 0000 GMT on the 20th. It had several characteristics of a warm front.

The C-D-E cloud band complex was associated with the most prominent disturbance in the isentropes but sloped northwestward with height and extended above 300 mb where its passage across Raoul I. occurred about 30 hours after the main disturbance near 550 mb. Strong vertical motions were probably partly responsible for that feature, and their origin is examined more fully in the next section.

A further point of importance in the analyses was the difficulty in fitting all the observations. This arose particularly at Raoul Island and Auckland, where the gradients necessary to fit the height observations greatly exceeded those implied by the observed winds. For example at Auckland at 0000 GMT 21 March the observed 1 km wind was 15 kt compared to a geostrophic wind of about 60 kt and the observed 1000-500 mb shear was 20 kt compared to 80 kt geostrophic. Therefore the

thermal advection at Auckland calculated using the geostrophic assumption was much greater than would have been the case if the observed winds were used. At Raoul Island the light winds observed were always at odds with the gradients implied by the height changes (Fig. 4).

A second problem is that the winds at a single level may not be representative of any substantial layer in the atmosphere. Figure 3a, for example, shows that frequently the winds at 500 mb were quite different from those at 400 or 600 mb. For our calculations, based on only two levels, it is essential to use winds representative of a 250 mb thick layer.

Therefore, in order to determine the large-scale patterns in practice, the winds should be averaged so that they are representative of a layer, not merely a single level, and then given equal weight with heights in the analysis. Consequently, the broad-scale (quasi-geostrophic) analyses in Fig. 2 do not slavishly fit the heights, except by including very small scale features as implied earlier. We have further established that the time section at a station for this case was not equivalent to a cross section at one instant. The degree to which extrapolation works is dependent on this equivalence and can probably be determined fairly well by assessing the lifetime of systems using satellite pictures.

4. Spiral cloud bands

With satellite pictures only every 12 hours it was difficult to trace the evolution and movement of the spiral cloud bands. Consequently it is possible that the bands may be incorrectly labelled in Fig. 2, especially if their lifetimes were shorter than suggested so that they were rapidly replaced by other bands.

The nature of the bands is difficult to determine. Cloud bands have been identified as common features ahead of warm fronts in mid-latitude depressions in the Northern Hemisphere (Elliott and Hovind 1964, Browning and Harold 1969, Browning et al. 1973) but these were all precipitating systems (see also the review by Harold and Austin 1974). House et al. (1976) identify six different types of rainband. Many studies have been made into the nature and characteristics of spiral bands in hurricanes (Ogura and Charney 1962, Anthes 1972, Kurihara and Tuleya 1974, Kurihara 1976, Diercks and Anthes 1976 a,b) and they have been clearly identified as internal inertia-gravity waves (see also reviews of tropical meteorology by Garstang 1972 and Anthes 1974). These waves arise from a form of dynamic instability, and grow through the barotropic conversion of mean azimuthal kinetic energy into eddy kinetic energy. Diercks and Anthes (1976a) found internal inertia-gravity waves mainly below the 450 mb level but only weakly discernible above there. Inertia-gravity waves of a larger scale have also been found in the tropical stratosphere and identified as Kelvin waves (Wallace and Kousky 1968).

All these features differ in several respects from the case here. Linear theory of internal gravity waves (Haltiner 1971 p 30, Holton 1972 p 173, and see Appendix C) can readily

handle only over-simplified model atmospheres. In this case, the cloud bands are embedded in a baroclinic atmosphere, the vortex is not axisymmetric, and Coriolis effects are probably of significance. However, even a cursory examination of Figs 3b and 4 shows several features which appear to be sinusoidal and continue for at least four cycles. Nevertheless, the geopotential height oscillations (Fig. 4) cannot be uniquely identified with the cloud bands although, as noted earlier, this may be because of aliasing since we cannot resolve periodicities of less than 24 hours in the height field, even if they were present. Similarly, changes in dew point depression at Raoul Island cannot be identified clearly with the bands except for the warm frontal character of Band B.

We have already noted the highly ageostrophic nature of the wind and height fields at Raoul Island, and a possible explanation for the cloud bands and perhaps the height oscillations (Fig. 4) is that they were caused by internal inertia-gravity waves, in the following manner.

A prominent feature of significance is the fairly continuous stable inversion layer near 500 mb (Fig. 3b) and since it was very dry above there (Fig. 3a), it indicates broadscale subsidence in the upper troposphere. However, between 500 and 600 mb there was a layer about 50-70 mb thick that was very close to the dry adiabatic lapse rate and at times was superadiabatic (at 1200 GMT on 19 and 20 March). One way in which such a layer might arise would be through the pronounced warm advection below 600 mb which was certainly present. Therefore, in this layer, $Ri \leq 0$, where Ri is the Richardson number, and as well as being statically unstable, such a layer would be unstable to Kelvin-Helmholtz waves (Chandrasekar 1961, Stone 1966) which are manifest as rolls perpendicular to the flow but occur on a very small scale. Internal gravity waves are also unstable in such a layer, and we therefore speculate as to whether the pronounced perturbations near 500 mb in the isentropes (Fig. 3b) originated from internal inertia-gravity waves which propagated upwards. Appendix C outlines the basic theory and characteristics of such waves.

5. Results

The vertical motions at 500 mb (ω_{500}) were computed using (3) and (4) with the smoothing operator (see Appendices A and B) applied once to the thickness equation and twice to the vorticity equation terms. Note that the vertical motions derived are the average for the whole 12-hour period and therefore are considerably blurred compared to the satellite picture.

Results from the thickness equation were more consistent and compared more favourably with the satellite pictures than results from the vorticity equation. This is because of the dominance of warm advection related processes and because the uncertainties in the analyses are reflected much more in the vorticity calculations (see Appendix B).

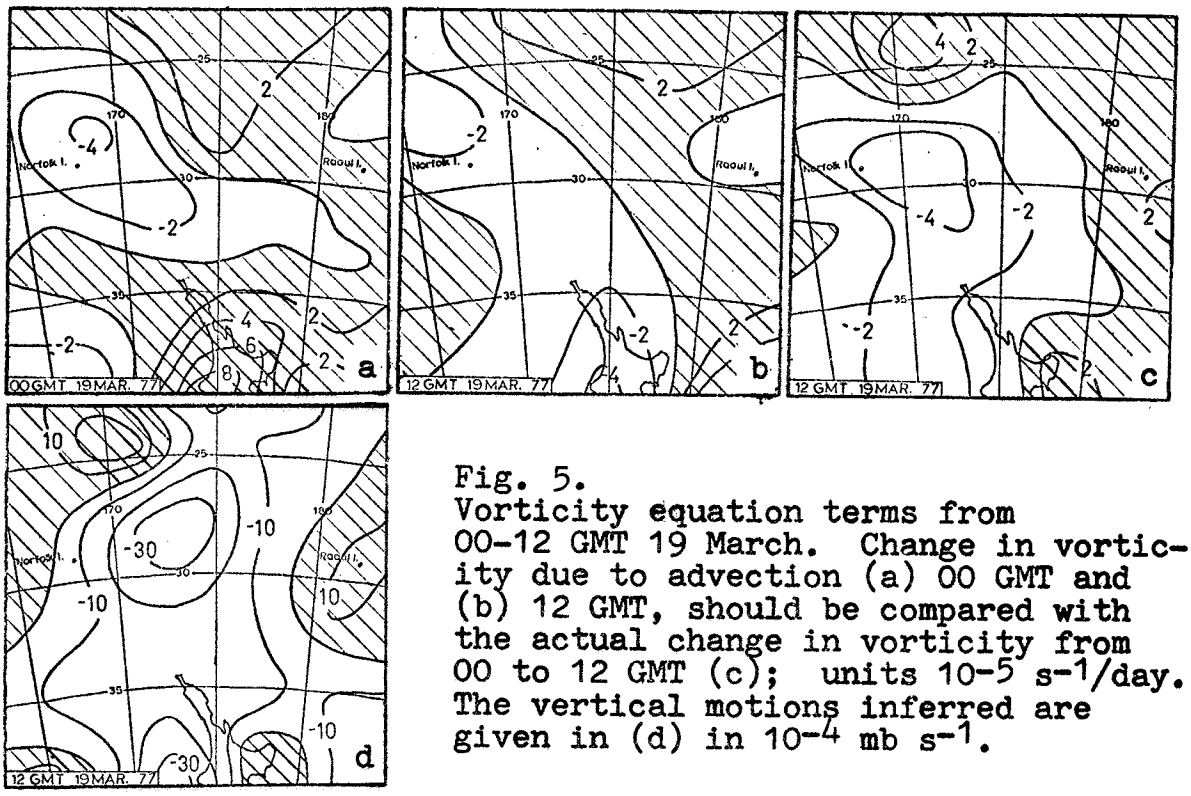

Fig. 5.
Vorticity equation terms from 00-12 GMT 19 March. Change in vorticity due to advection (a) 00 GMT and (b) 12 GMT, should be compared with the actual change in vorticity from 00 to 12 GMT (c); units 10^{-5} s^{-1}/day. The vertical motions inferred are given in (d) in 10^{-4} mb s^{-1}.

Figure 5 shows the results for 0000-1200 GMT 19 March from the vorticity equation. The change in vorticity due to advection (a) at 0000 GMT and (b) at 1200 GMT should be compared with (c) the actual change in vorticity. Advection goes only part way to explaining the vorticity change, and therefore upward motion and the associated convergence generate the rest (d). The contribution of surface friction to thickness change is given in Figs 6b and 6c, and the contribution to vertical motion has an identical pattern, but less by a factor of 4.4 (to be in units of 10^{-4} mb s^{-1}). Therefore the maximum value was 9 x 10^{-4} mb s^{-1}. Consequently, the patterns of convergence and generation of cyclonic vorticity follow the areas of upward motion in Fig. 5d fairly closely.

Figure 6 shows the contributions from the terms in the thickness equation, as they pertain to changes in the thickness $Z_{500} - Z_{1000}$, where Z is the height. Thus changes due to thickness advection (c), (f), and latent heat (a), (d) each contribute over 100 m/day to warming south and east of Norman whereas the actual change in thickness (g) is quite small in that area. Therefore upward motion (h) was present to compensate for the warming. In the south, where a cold front moved rapidly eastwards across New Zealand (Figs 2a, d), the cold advection (Fig. 6 (c), (f)) largely explained the actual cooling (g) and vertical motions were small. Surface friction effects were relatively small but contribute to cooling above

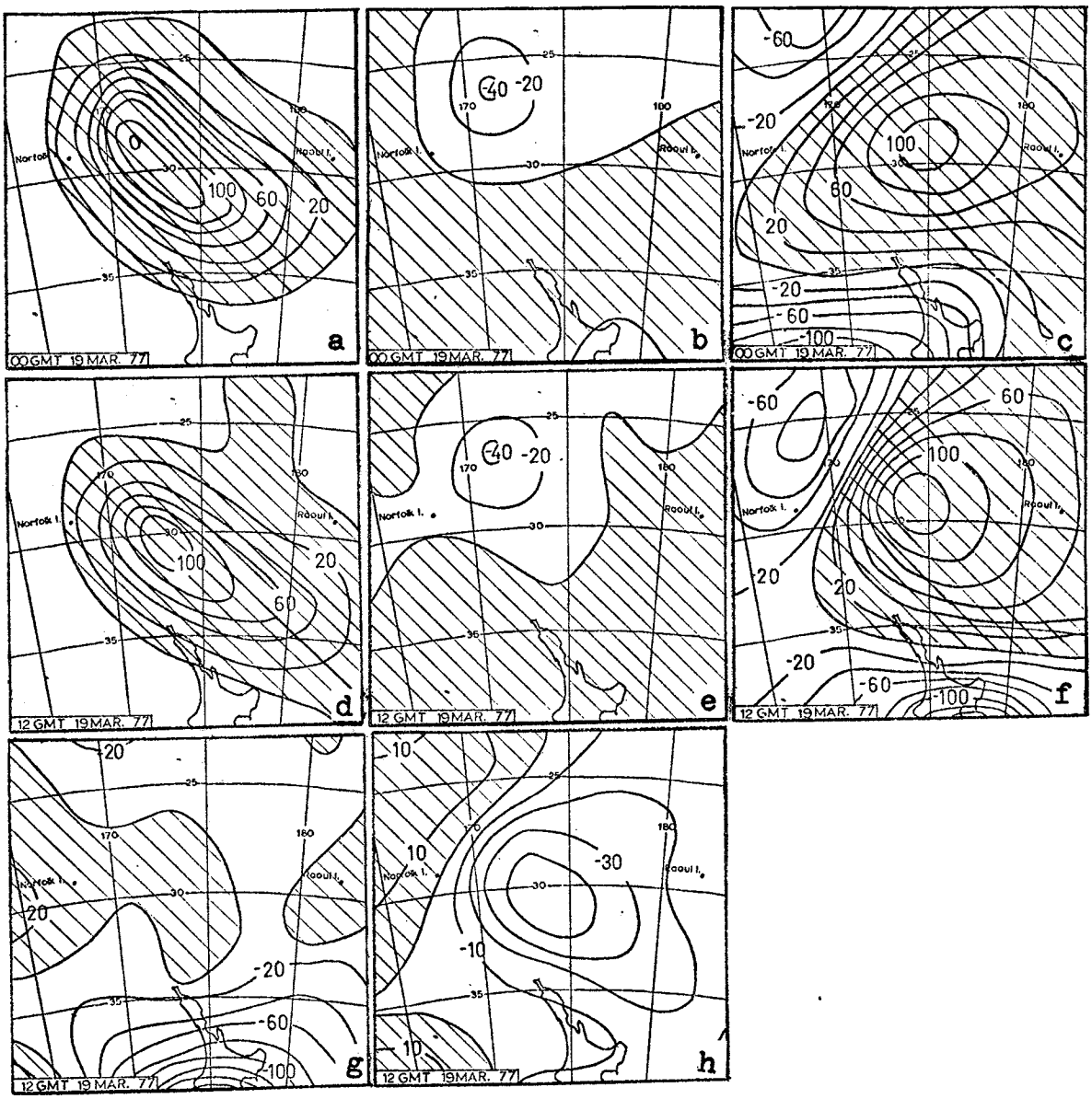

Fig. 6. Contributions from the terms in the thickness equation from 00-12 GMT 19 March. Change in thickness due to latent heat release (a) 00 GMT and (d) 12 GMT; surface friction vertical motion (b) 00 GMT and (e) 12 GMT; and advection (c) 00 GMT and (f) 12 GMT; should be compared with the observed change from 00-12 GMT (g); units m/day. The inferred vertical motions are given in (h) in 10^{-4} mb s^{-1}.

the surface low.

There is a broad agreement between the calculated omegas, Figs 5d and 6h, with each other and with the satellite picture, Fig. 2f. Possibly this could be improved by using different expressions for the rainfall rate, Eq. (8), and by increasing the value of C_D used in (6). These allow the latent heat release and surface friction contributions to be adjusted independent of the other calculations. The largest discrepancy was from 0000 to 1200 GMT 20 March, when there was a cooling at Auckland and west of there (e.g. 37°S 170°E) in spite of the warm advection, yet the implied vertical motion is not observed to be very marked in the satellite pictures. Partly, this arises from uncertainties in the analyses, but it also appears that some widespread vertical motion cooling can occur without the development of major cloud sheets. This is especially so, of course, in very dry air. However, the main upward motion was correctly determined to be south and southeast of the centre of the vortex, and since the movement southwards of Norman was built into these calculations it is possible to explain that movement.

Similar patterns to those in Figs 5 and 6 were found in the calculations for the other periods. Therefore only the vertical motion patterns deduced from the thickness equation are presented in Fig. 7 for (a) 1200 GMT 19 to 0000 GMT 20 March, (b) 0000-1200 GMT 20 March and (c) 1200 GMT 20 to 0000 GMT 21 March. Reasonable agreement exists with the satellite pictures (Fig. 2).

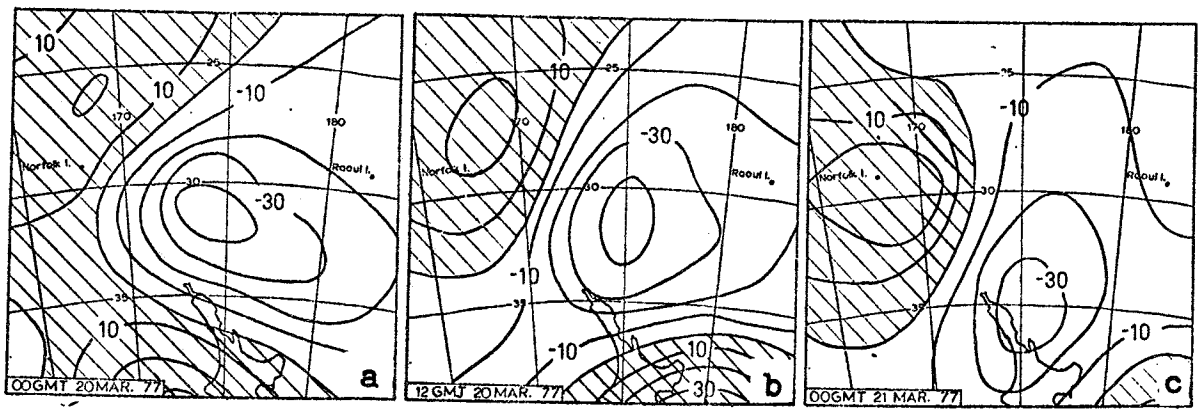

Fig. 7 Deduced vertical motions from the thickness equation for (a) 12 GMT 19th - 00 GMT 20 March; (b) 00-12 GMT 20 March; (c) 12 GMT 20th - 00 GMT 21 March; 10^{-4} mb s^{-1}

6. Discussion

The common concept of a steering field utilises heavily smoothed fields averaged in the vertical which, in this case, would produce a northwesterly steering current over Norman. However, Norman was a shallow feature with little effect above 500 mb and the steering field should be weighted accordingly. The 750 mb field heavily smoothed, in fact, does give a light northerly component over Norman and, as shown in Figs 5a and 6, the main area of cyclonic vorticity advection was south and southwest of the vortex centre. This was, however, a minor factor in the overall movement of the storm.

The strong upward motion south and southeast of the vortex was almost entirely due to the pronounced warm advection supplemented by latent heating. In other words, to a first approximation for this case we have simplified (2) to

$$\sigma\omega = -\underline{v}.\nabla\frac{\partial\phi}{\partial p} - \frac{\kappa Q}{p} \qquad (9)$$

Vorticity advection contributed little to the vertical motions.

As a result of this mid-tropospheric upward motion, cyclonic vorticity was generated to the south and southeast of the vortex centre (Fig. 5c), and brought surface pressure and 500 mb height falls into that area. Southwest of the vortex the cyclonic vorticity advection nearly balanced the actual change. However, elsewhere, in effect, we have simplified (1) to

$$\frac{\partial\zeta}{\partial t} = f_0\frac{\partial\omega}{\partial p} \qquad (10)$$

An important aspect of these developmental processes which were responsible for the southward movement of the storm is that they were always taking place away from the actual vortex centre and therefore it was not possible for the storm to intensify or deepen.

The main indicators of the storm's movement and intensity were the strong vertical motions apparent from the satellite picture due south of the vortex centre, with the steering field only a minor factor. The strong vertical motions were also indicated by the small changes in thickness taking place in spite of substantial warm advection. The other factor which must be considered is the vorticity advection field which was not contributing to changes in a substantial manner. Both these features appear to be quite common in low latitude storms.

A question remains as to why the thickness does not

respond to the warm advection and produce a warm tongue as it typically does in mid-latitude storms. The latter evolve through several clearly defined stages as they grow, mature, and occlude, and their life is therefore limited. In contrast, low latitude storms (not just this case) frequently seem to exist for several days embedded in or on the fringe of a baroclinic zone, but with the warm and cold advection producing little net effect on the thermal field. Apparently the thermal advection is largely compensated for immediately by vertical motions.

Erickson and Winston (1972) investigated the interaction of tropical storms with the mid-latitudes by compositing cases where major cloud band connections occurred. They suggest that the injection of heat and moisture into middle latitudes by such systems plays a major role in the build up of the autumnal circulation. They also outlined the northern hemispheric energetics accompanying such events and show an increase in both zonal and eddy kinetic energy for up to a week following the cloud band connections.

The key may lie in the question of what determines whether a storm is "low-latitude" or "mid-latitude" in nature. The answer seems to be related to whether the storm is equatorward of the subtropical jet stream and/or embedded in surface easterlies. These two factors are correlated.

The low-latitude storms may or may not have their origin as tropical cyclones, but several features are common to both. Radiational heating of the sea surface produces evaporation which is converted into heating of the atmosphere through subsequent release of latent heat by these storms. However, the transport of warm air poleward by advection, and the latent heating, are largely offset by upward motions and do not therefore contribute much to warming in the area of the storm. Rather, the warming occurs in the subsidence, frequently in the anticyclone to the south. This meridional overturning creates zonal kinetic energy in mid-latitudes in addition to the eddy kinetic energy associated with the storm itself, and since the storm is embedded in surface easterlies which provide a source of westerly momentum through surface friction, the meridional overturning also transports westerly momentum into the subtropical jet stream to the south. Thus the important difference between low-latitude and mid-latitude storms may be in whether there is a source or sink of momentum at the surface and whether it is redistributed by meridional or eddy processes. This speculation cannot be resolved here, but is put forward as a topic for future research. We further speculate that the breakdown in the character of the low-latitude storm occurs with the approach of a disturbance in the westerlies so that vorticity advection becomes of significance.

7. Conclusions

Although the methods used in this study were successful to a certain extent, in hindsight the procedure is not to be recommended in general. In particular, the use of only two levels, 1000 and 500 mb, to determine what was going on, is too great a simplification and diagnostic studies would be

better to use as many levels as possible. Simplifications can then be made after the calculations have been performed and the importance of various quantities is known. In the case under investigation it was perhaps fortunate that the trends at 1000 mb and 500 mb were similar since more detailed vertical resolution is essential to separate out the causes of opposite changes. The other main objection to the current method is the assumption that quasi-geostrophic motion is most important. In general this should be the case, but it would be preferable if the ageostrophic terms were assessed and eliminated after it had been shown that they were negligible. Unfortunately, to do this properly, a very much denser network of observations is needed, as we saw from the observations at Raoul I., and in the New Zealand area this is not achieved.

An excellent model for a study of this nature is presented by Krishnamurti (1968a) and applied to examples by Krishnamurti (1968b). The latter study demonstrates the importance of non-geostrophic terms although thermal and vorticity advection and latent heating terms appear to be most important.

In this case study the analyses almost certainly contain errors but it does not seem possible to improve them without extra observations. The Australian analyses were no help in spite of any benefits from satellite sounding data that may have been available, since their 0000 and 1200 GMT analyses were inconsistent with each other and clearly incorrect.

In preparing the analyses we found it necessary to determine from the satellite pictures the approximate lifetimes of systems in order to assess the validity of steady state assumptions that would allow an equivalence between cross-sections at one instant with time sections at one station to be assumed. At Raoul I. the short life times did not allow such an equivalence to be established. We also found the observations at Raoul I. and Auckland to be highly ageostrophic, and in assessing the broadscale geostrophic flow it was necessary to give equal weight to both the height and the wind field, and to ensure that the winds were representative of a layer rather than a single level.

The spiral bands crossing Raoul Island also posed analysis problems and it was suggested that they may have been related to internal inertia-gravity waves.

Calculations of vertical motions in the mid-troposphere based on the thermodynamic equation and the vorticity equation gave results in sufficient agreement with each other and with the satellite pictures to enable some conclusions to be drawn about the main processes going on. However the residual errors in the vorticity equation are apparently so large that it is of doubtful use for this purpose by itself.

The strong upward motions south and southeast of tropical cyclone Norman were mostly due to warm advection supplemented by latent heating. As a result, cyclonic vorticity was generated and brought surface pressure and 500 mb height falls into that area, and the vortex moved southwards. Thus the presence of strong upward motions, as indicated by clouds in

satellite photographs, should be used as a primary indication of the effects of development on movement.

The tropical storm Norman was classified as a not uncommon 'low-latitude' type storm which has several characteristic features. These are the presence of cloud bands to the south and southeast which indicate that latent heating and warm advection are almost immediately offset by vertical motion cooling, and the system does not occlude in the mid-latitude sense. We speculated as to whether the characteristics of such storms were related to their location north of the subtropical jet stream and embedded in surface easterlies, so that momentum fluxes were an important factor. This would be a good topic for future work.

References

Anthes, R.A., 1972: The development of asymmetries in a three dimensional numerical model of the tropical cyclone. Mon. Wea. Rev., 100, 461-476.

Anthes, R.A., 1974: The dynamics and energetics of mature tropical cyclones. Rev. Geophys. Space Phys., 12, 495-522.

Browning, K.A. and F.W. Harrold, 1969: Air motion and precipitation growth in a wave depression. Quart. J. Roy. Met. Soc., 95, 288-309.

Browning, K.A., M.E. Hardman, T.W. Harrold and C.W. Pardoe, 1973: The structure of rainbands within a mid-latitude depression. Quart. J. Roy. Met. Soc., 99, 215-231.

Chandrasekhar, S., 1961: Hydrodynamic and Hydromagnetic Stability. International series of monographs on physics. Clarendon Press, Oxford, 652 pp.

Diercks, J.W. and R.A. Anthes, 1976a: A diagnostic study of spiral bands in a nonlinear hurricane model. J. Atmos. Sci., 33, 959-975.

Diercks, J.W. and R.A. Anthes, 1976b: A study of spiral bands in a linear model of a cyclonic vortex. J. Atmos. Sci., 33, 1714-1729.

Elliott, R.D. and R. Hovind, 1964: On convection bands within Pacific Coast storms and their relation to storm structure. J. App. Met., 3, 143-154.

Erickson, C.O. and J.S. Winston, 1972: Tropical storm, mid-latitude cloud band connections and the autumnal buildup of the planetary circulation. J. App. Met., 11, 23-36.

Garstang, M., 1972: A review of hurricane and tropical meteorology. Bull. Amer. Met. Soc., 53, 612-630.

Haltiner, G.J., 1971: Numerical Weather Prediction. John Wiley & Sons, New York. 317 pp.

Harold, T.W. and P.M. Austin, 1974: The structure of precipitation systems - a review. J. Recherches Atmospheriques, 8, 41-57.

Holton, J.R., 1972: An Introduction to Dynamic Meteorology. International Geophysics Series. Academic Press, New York.

Houze, R.A., Jr, P.V. Hobbs, K.R. Biswas and W.M. Davis, 1976: Mesoscale structure of rainfall in occluded cyclones. Proc. of the Sixth Conf. on weather forecasting and analysis. May 10-13, 1976. Albany, New York. Amer. Met. Soc. 310-317.

Krishnamurti, T.N., 1968a: A diagnostic balance model for studies of weather systems of low and high latitudes, Rossby number less than 1. Mon. Wea. Rev., 96, 197-207.

Krishnamurti, T.N., 1968b: A study of a developing wave cyclone. Mon. Wea. Rev., 96, 208-217.

Kurihara, Y., 1976: On the development of spiral bands in a tropical cyclone. J. Atmos. Sci., 33, 940-958.

Kurihara, Y. and R.E. Tuleya, 1974: Structure of a tropical cyclone developed in a three dimensional numerical simulation model. J. Atmos. Sci., 31, 893-919.

May, A.I. and J.W. Kidson, 1971: The objective prediction of cloud and precipitation. N.Z. Met. S. Tech. Note 203.

Obrien, J.J., 1970: Alternative solutions to the classical vertical velocity problem. J. App. Met., 9, 197-203.

Ogura, Y. and J.G. Charney, 1962: A numerical model of thermal convection in the atmosphere. Proc. of the International Symp. on NWP. Tokyo, Japan. Nov. 7-13, 1960. Met. Soc. Japan, 431-451.

Stone, P.H., 1966: On non-geostrophic baroclinic stability. J. Atmos. Sci., 23, 390-403.

Trenberth, K.E., 1973: A five layer numerical weather prediction model. N.Z. Met. S. Tech. Note 222.

Trenberth, K.E., 1977: Objective numerical analysis in New Zealand. N.Z. Met. S. Tech. Inf. Circ. 158.

Vincent, D.G., K.E. Bossingham and H.J. Edmon, Jr, 1976: Comparison of large scale vertical motions computed by the kinematic method and quasi-geostrophic omega-equation. Proc. of the Sixth Conf. on weather forecasting and analysis. May 10-13 1976, Albany, New York. Amer. Met. Soc., 357-364.

Wallace, J.M. and V.E. Kousky, 1968: Observational evidence of Kelvin waves in the tropical stratosphere. J. Atmos. Sci., 25, 900-907.

APPENDIX A

Finite Differences

By comparing the actual change between 0000 and 1200 GMT with the average of the various terms on the RHS at 0000 and 1200 GMT, we are using a trapezoidal implicit finite differencing scheme. This scheme may be used for integrating the equations, but here the actual rather than predicted fields are used. It is computationally stable for linear advection, with no computational mode and no amplification or reduction in amplitude but it does retard all waves, and this error determines the minimum resolution and therefore the degree of smoothing desirable.

Consider the advection equation:

$$\frac{\partial F}{\partial t} = - \underline{v} . \nabla F \qquad \text{(A1)}$$

For the 1 dimension linear case, where

$$x = m \Delta x$$

$$t = n \Delta t$$

The trapezoidal scheme solves

$$\frac{F_{m,n+1} - F_{m,n}}{\Delta t} = -\frac{c}{2}\left(\frac{F_{m+1,n+1} - F_{m-1,n+1}}{2\Delta x} + \frac{F_{m+1,n} - F_{m-1,n}}{2\Delta x} \right) \qquad \text{(A2)}$$

where c is the speed.

The analysis of this scheme (see Haltiner 1971, p. 99) assumes a solution of the form

$$\left.\begin{aligned} F &= B^{n\Delta t} e^{i\mu m \Delta x} \\ \text{with } F &= A e^{i\mu x} \quad \text{at} \quad t = 0 \end{aligned}\right\} \qquad \text{(A3)}$$

and finds a solution

$$\left.\begin{aligned} F_{m,n+1} &= A\, e^{i(\mu m \Delta x - 2n\theta)} \\ \text{where} \quad \theta &= \arctan\left(\frac{c\Delta t}{2\Delta x} \sin \mu \Delta x \right) \end{aligned}\right\} \qquad \text{(A4)}$$

which must be compared with the correct solution

$$\left.\begin{aligned} F_{m,n+1} &= A\, e^{i(\mu m \Delta x - 2n\theta')} \\ \text{where} \quad \theta' &= \frac{\mu c \Delta t}{2} \end{aligned}\right\} \qquad \text{(A5)}$$

Therefore the effect of this scheme is to retard all waves, and the ratio of the calculated to correct phase speed is given by

$$\frac{\theta}{\theta'} = \frac{\arctan\left(\frac{c\Delta t}{2\Delta x}\sin\mu\Delta x\right)}{\frac{\mu c\Delta t}{2}} \qquad (A6)$$

If we put $\mu = \frac{2\pi}{n\Delta x}$

where $n\Delta x$ is the wavelength

and assume Δt = 12 hours

Δx = 200 km

then the percentage error (=(1- θ/θ')x 100) as a function of the phase speed, c, is given for various wavelengths in Table A1.

Table A1: Error in speed of wave of given wavelength, (= $n\Delta x$) expressed as a percentage of the correct speed.

Wavelength	n	Phase Speed 5	10	20	30 ms^{-1}
400	2	100	100	100	100
600	3	61.3	66.8	76.1	81.9
800	4	41.6	51.4	66.5	75.0
1200	6	22.6	33.5	52.3	63.8
1600	8	14.0	23.1	41.5	54.4
2000	10	9.4	16.6	33.5	46.6
3000	15	1.7	6.0	18.7	31.0

For the case being investigated, wind speeds at 500 mb exceed 30 ms^{-1} at isolated places, and smoothed fields averaged 20 ms^{-1} over large areas. However several small scale traceable features with large amplitude moved at much slower speeds. A demand for at least 50% accuracy in movement restricts the resolution to 1400 km (n = 7) for 20 m s^{-1} speeds, or 700 km (n = $3\frac{1}{2}$) for 5 m s^{-1} speeds.

It was therefore desirable to use smoothing techniques and consider only the broader scales of greater than 1000 km wavelength.

APPENDIX B

Smoothing

As shown in the previous section, greatest errors occur in the short wavelengths, and it is desirable to remove $2\Delta x$ waves altogether. The following 9-point smoothing operator will be used to achieve this.

$$\bar{f}_0 = f_0 + \tfrac{1}{8}(f_2 + f_4 + f_6 + f_8 - 4f_0) + \tfrac{1}{16}(f_1 + f_3 + f_5 + f_7 - 4f_0) \qquad \text{(B1)}$$

where the grid point configuration is given in Fig. B1.

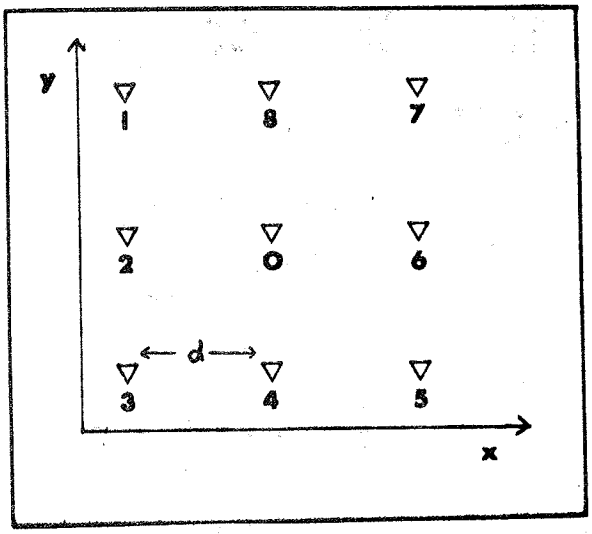

Fig B1. The grid point configuration for smoothing.

This has a response function given by

$$R = \frac{\bar{A}}{A} = \tfrac{1}{4}(\cos rd + \cos sd) + \tfrac{1}{2}(\cos rd \cos sd)$$

where $r = \frac{2\pi}{L_x}$, $s = \frac{2\pi}{L_y}$. (B2)

For Lx = Ly = nd, this reduces the amplitude of waves by 100% for n = 2, 94% for n = 3, 75% for n = 4 and 44% for n = 6. For Lx = ∞, Ly = nd it reduces the amplitude by 100% for n = 2, 75% for n = 3, 50% for n = 4 and 25% for n = 6.

Since we use vorticity, which involves the del squared operator, short wavelengths are enhanced at the expense of long waves by a factor of $\frac{1}{r^2 + s^2}$. Therefore, it is necessary to apply greater smoothing to the vorticity equation terms and the accuracy is less owing to the poor resolution of short waves through inadequate data.

APPENDIX C

Internal inertia-gravity waves

Consider a basic current in the east-west direction at constant velocity $\bar{u}$, then a perturbation analysis $u = \bar{u} + u'$ etc, gives the following set of equations, where we drop the primes.

$$\frac{\partial u}{\partial t} + \bar{u}\frac{\partial u}{\partial x} - fv + \frac{\partial \phi}{\partial x} = 0 \qquad \text{(C1)}$$

$$\frac{\partial v}{\partial t} + \bar{u}\frac{\partial v}{\partial x} + fu + \frac{\partial \phi}{\partial y} = 0 \qquad \text{(C2)}$$

$$\frac{\partial u}{\partial x} + \frac{\partial v}{\partial y} + \frac{\partial \omega}{\partial p} = 0 \qquad \text{(C3)}$$

$$\frac{\partial}{\partial t}\frac{\partial \phi}{\partial p} + \bar{u}\frac{\partial}{\partial x}\frac{\partial \phi}{\partial p} + \sigma\omega = 0 \qquad \text{(C4)}$$

If we assume a solution of the form

$$u = u(y)\, e^{i[k(x-ct) + \lambda p]} \quad \text{etc.}$$

then we get:

$$ik(\bar{u}-c)u - fv + ik\phi = 0 \qquad \text{(C5)}$$

$$ik(\bar{u}-c)v + fu + \frac{\partial \phi}{\partial y} = 0 \qquad \text{(C6)}$$

$$iku + \frac{\partial v}{\partial y} + i\lambda\omega = 0 \qquad \text{(C7)}$$

$$ik(\bar{u}-c)i\lambda\phi + \sigma\omega = 0 \qquad \text{(C8)}$$

This reduces to an equation of the form

$$\frac{\partial^2 v}{\partial y^2} + l^2 v = 0 \qquad \text{(C9)}$$

where $$l^2 = \frac{\lambda^2 k^2(\bar{u}-c)^2 - (\sigma k^2 + \lambda^2 f^2)(\bar{u}-c) + \sigma\beta}{\sigma(\bar{u}-c)}$$

and $$\beta = \frac{df}{dy} \text{ is constant.} \qquad \text{(C10)}$$

Therefore $v = A_1 e^{il_y} + A_2 e^{-il_y}$ (C11)

and from (C10)

$$(\bar{u}-c)^3 - \left[\frac{\sigma(k^2+l^2)}{\lambda^2 k^2} + \frac{f^2}{k^2}\right](\bar{u}-c) + \frac{\sigma\beta}{\lambda^2 k^2} = 0 \qquad \text{(C12)}$$

Solution of this cubic gives the phase speed of the wave.

The general solution is complicated, and it is easier to look at several cases.

Case I. $\lambda = 0$. In this case the vertical wavelength is infinite, there is no divergence, and (C12) reduces to the Rossby wave formula

$$\bar{u} - c = \frac{\beta}{k^2+l^2} \qquad \text{(C13)}$$

Case II. For short horizontal wavelengths, say about 100 km, the last term in (C12) is negligible, and the second term in the bracket is small, so that

$$\left.\begin{aligned} \bar{u} - c &\approx 0 \\ \text{and} \quad \bar{u} - c &\approx \pm \left[\frac{\sigma}{\lambda^2}\,\frac{k^2+l^2}{k^2}\right]^{\frac{1}{2}} \end{aligned}\right\} \qquad \text{(C14)}$$

The latter solutions are those for internal gravity waves.

Case III. If λ is large - for very short vertical wavelengths ($<<$ 100 mb), the last term is again negligible and the first term in the bracket is small, so that

$$\left.\begin{aligned} \bar{u} - c &\approx 0 \\ \text{and} \quad \bar{u} - c &\approx \pm \frac{f}{k} \end{aligned}\right\} \qquad \text{(C15)}$$

and the latter are pure inertial waves.

Case IV. For mesoscale features with horizontal wavelengths 300-1000 km, the last term is still small and approximate solutions are

$$\left.\begin{aligned} \bar{u} - c &\approx \frac{\beta}{(k^2+l^2) + \frac{f^2\lambda^2}{\sigma}} \\ \text{and} \quad \bar{u} - c &\approx \pm\left[\frac{\sigma}{\lambda^2}\,\frac{k^2+l^2}{k^2} + \frac{f^2}{k^2}\right]^{\frac{1}{2}} \end{aligned}\right\} \qquad \text{(C16)}$$

The first solution corresponds to the modified Rossby wave, where $\omega \approx 0$. The second and third solutions are internal inertia-gravity waves.

For typical values at 30°S we take

$\beta = 1.9 \times 10^{-11}$ $m^{-1}s^{-1}$

$f = -.7 \times 10^{-4}$ s^{-1}

$\sigma = 2 \times 10^{-2}$ $m^2\ mb^{-2}\ s^{-2}$

$k = l = 2\pi/4 \times 10^5$ m^{-1} (horizontal wavelength 400 km)

$\lambda = 2\pi/150$ mb^{-1} (vertical wavelength 150 mb≈2km)

then $\bar{u} - c \approx .03$ m s^{-1}

and $\bar{u} - c \approx \pm 6.5$ m s^{-1}

The period of the latter waves is 17 hours.

These waves propagate at a speed c relative to the basic current. Their main characteristics are that subsidence takes place ahead of the warm tongue and upward motion ahead of the cold tongue, thereby producing adiabatic warming and cooling which causes the temperature field to propagate. Geopotential heights are consistent with the hydrostatic equation and local gradients are set up which maintain the wave motion. A westward slope with height of a perturbation indicates a downward energy and momentum propagation.

The above solutions are still grossly oversimplified. For instance the static stability is a function of pressure and vertical shear should be included in the basic current. In the case study, there were easterlies at low levels and westerlies aloft (Fig. 3a). Vertical shear has a destabilising effect on the waves. However, there are several other terms that could also be important on a mesoscale and we cannot confirm that the phenomena crossing Raoul I. were internal inertia-gravity waves.